TÜBİTAK

Turkish Journal of Earth Sciences

http://journals.tubitak.gov.tr/earth/

Research Article

Turkish J Earth Sci
(2019) 28: 882-901

doi:10.3906/yer-1902-1

Mineralogy, alteration, and sulfur isotope geochemistry of the Zehabad intermediate-sulfidation epithermal deposit, NW Iran

Somaye SHAHBAZI[1], **Majid GHADERI**[1,*], **Pura ALFONSO**[2]

[1]Department of Economic Geology, Tarbiat Modares University, Tehran, Iran

[2]Department of Mining, Industrial and ICT Engineering, Polytechnic University of Catalonia, Barcelona, Spain

Received: 01.02.2019 • **Accepted/Published Online:** 13.09.2019 • **Final Version:** 07.11.2019

Abstract: The Zehabad Pb-Zn-Au-Ag (Cu) deposit lies in the Alborz magmatic arc of northwestern Iran. Ore-bearing breccia veins hosted by Eocene tuffs emplaced along the 80–130° trending fault and fracture zone. Mineralization occurs in the contact of the late Eocene igneous bodies and the Eocene volcanic and volcanosedimentary Karaj Formation. Mineralization formed in five stages: 1) disseminated framboidal pyrite and minor chalcopyrite and sphalerite; 2) quartz veins containing chalcopyrite, bornite, pyrite, and sphalerite; 3) deposition of specularite and gold grains hosted in quartz veins that crosscut chalcopyrite; 4) the main stage of mineralization that contains galena, sphalerite, tennantite-tetrahedrite, pyrite, sulfosalts, and gold; 5) barren quartz-calcite veins with sulfide mineral fragments of earlier stages. The hydrothermal alteration from closest to the veins outwards includes: a) silicification; b) phyllic with quartz, pyrite, sericite, and calcite; c) argillic with illite, kaolinite, and montmorillonite; d) propylitic containing epidote, calcite, chlorite, and sericite and; e) carbonatization that crosscuts all previous alteration types. Quartz and calcite are the most important gangue minerals at the deposit and show a close relationship with mineralization. Sulfur isotope compositions (0.8‰ to −10.1‰) suggest that the ore-forming fluids derived from magmatic sources with a temperature range of 276–288 °C. According to the field (macroscopic), microscopic, alteration, and sulfur isotope studies, the Zehabad base and precious metal mineralization is considered an intermediate-sulfidation epithermal deposit.

Key words: Epithermal, intermediate-sulfidation, sulfur isotopes, Zehabad, Alborz, Iran

1. Introduction

A number of epithermal deposits occur within the Tarom-Hashtjin subzone of the Western Alborz-Azerbaijan volcano-plutonic arc in NW Iran (Nabavi, 1976). Tarom-Hashtjin is composed of Eocene volcanic and volcanosedimentary rocks that formed in a back-arc basin (Vincent et al., 2005; Guest et al., 2006; Zanchi et al., 2006; Ballato et al., 2010, 2017, Verdel et al., 2011; Asiabanha and Foden, 2012; Madanipour, 2013), which were then cut and altered by late Eocene high-K calc-alkaline to alkaline intrusive bodies (Castro et al., 2013; Nabatian et al., 2014, 2016). Some examples of epithermal deposits in the subzone are Ghonchekhoran, Najafabad, Somagh, Nikoueieh (Pb-Zn-Cu±Au, Ag) (Aghajani Marsa et al., 2015), Abbasabad (Cu) (Moradi et al., 2010; Jahandideh Kazempour et al., 2011; Moradi, 2011), Khalifelou (Cu) (Esmaeli et al., 2015) Goloujeh (polymetallic epithermal deposit) (Mehrabi et al., 2016), Aghkand (base metal) (Kouhestani et al., 2017), Aliabad-Khanchay (base metal) (Kouhestani et al., 2018), and Chodarchay (Cu-Au) (Yasami et al., 2017, 2018) (Figure 1). The deposits are mainly hosted by Eocene tuffs and volcanic rocks and in some places by late Eocene plutonic rocks. The Zehabad deposit is the only active base and precious metal mine in the southern part of the Tarom-Hashtjin subzone. It is located 57 km northwest of Qazvin, in northwestern Iran (Figure 1). The mineralization at the deposit is mainly hosted in breccia veins. There were 30 ore-bearing veins at Zehabad deposit. Mining at Zehabad took place between 1959 and 1977 and then restarted in 2010.

The Ghara-Katala and Ghara-Changol veins were operated during 1959–1977. The Ghara-Katala vein is still under exploitation and contains 150,000 tons of Pb and Zn grading 7.7 wt.% Pb+Zn. The galena concentrate contains 8 ppm Au and 600 ppm Ag (Amin Khorramdasht Exploration Company, 2006; unpublished company report).

Except for geological mapping studies on the scale of 1:250,000 (Stocklin and Eftekharnezhad, 1969), a few unpublished company exploration reports (Amin

* Correspondence: mghaderi@modares.ac.ir

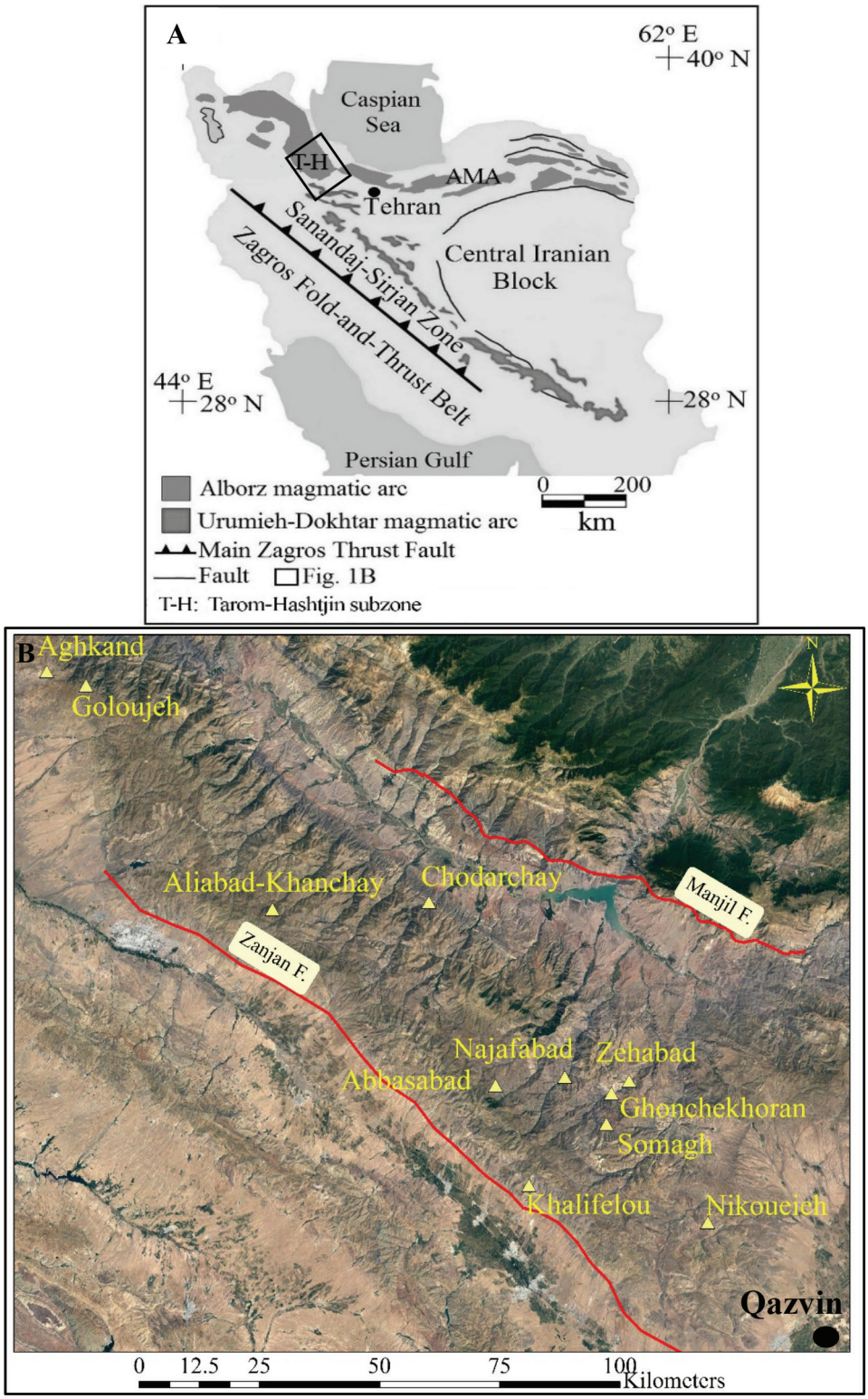

Figure 1. A) Location of the Tarom-Hashtjin subzone in the Alborz-Azerbaijan Magmatic Belt (NW Iran) and Zehabad deposit (Nabavi, 1976). B) Locations of some examples of Tarom epithermal deposits between Zanjan and Manjil Faults.

Khorramdasht Exploration Company, 2006; unpublished company report), and the preliminary studies of Khodaparast (2002), there are no comprehensive studies focusing on the type of ore deposition at Zehabad. In this paper, characteristics of the Zehabad deposit are discussed including the petrography of host Eocene lavas and tuffs as well as late Eocene intrusive rocks, structural observations, ore mineralogy, types of alteration, and sulfur isotope compositions of sulfide minerals to determine the genesis and mineralization styles.

2. Materials and methods

During the field survey, 300 samples were collected from the outcrops and tunnels. Also, 370 samples were selected from 600 m of cores. Petrography and alteration observations on the Zehabad rocks are based on the study of 156 thin sections, including 60 sections from the drill cores, 11 sections from the tunnels, and 85 sections from the outcrops. Mineralization, texture, and structure, as well as paragenetic survey, are based on 13 thin-polished sections from the surface and 37 thin-polished samples from the tunnels.

Sulfur isotope values of the Zehabad deposit were measured in 7 galena, 13 sphalerite, and 6 chalcopyrite samples collected from levels 1, 3, and 5 of the Ghara-Changol mine and levels 5, 6, 8, and 9 of the Ghara-Katala mine. Due to the failure in distinguishing between different stages of pyrite, this mineral was not found suitable for sulfur isotope analysis. Mineral aggregates were picked up using tweezers and were crushed to grains of 0.1–0.5 mm in size. Clean sulfide grains were then handpicked under a binocular microscope. These samples were analyzed using a Delta-C Finnigan MAT continuous-flow isotope-ratio mass spectrometer with a thermal conversion-elemental analyzer (TC-EA). The analyses were performed at the facilities of the Scientific and Technological Services of the University of Barcelona, Spain. The results are given as $\delta^{34}S$ values relative to the Vienna Canyon Diablo Troilite standard (V-CDT). The analytical accuracy is within ±0.1‰ at σ1.

3. Geology of the Zehabad deposit

The Zehabad deposit is located 57 km northwest of Qazvin, NW Iran (Figure 1). It is hosted by an Eocene volcanic complex that formed due to shallow submarine explosive eruptions to more effusive subaerial eruptions in a back-arc environment (Vincent et al., 2005; Guest et al., 2006; Zanchi et al., 2006; Ballato et al., 2010, 2017; Verdel et al., 2011; Asiabanha and Foden, 2012; Madanipour, 2013).

The main stress in the Zehabad area is related to the Zanjan Fault with a NE dip and the Zehabad host rocks thrust toward this fault. The Manjil Fault forms a similar situation in the northern units (Figure 1). The Pachichay (or Pachi River) resulted from a tension fracture that has a 40° angle relative to the Zanjan-Manjil Fault Zone and its parallel river set. Geologic evidence and the presence of a left-lateral strike-slip component in some faults show that the main stress at the Zehabad deposit was compressional. A total of 297 faults and 126 fractures were recognized at the deposit, which can be divided into two main fault and fracture zones. The first zone has a 20–40° trend, such as the Pachi River Fault. The second zone has a 120–150° trend. These steeply dipping (85–90°) zones do not show any transverse displacement. The Ghara-Changol and Ghara-Katala veins are parallel to the second fault and fracture zone. The Ghara-Changol vein system postdates the main branch of the Kamran-Darreh Fault (Figure 2). These fault zones have been active throughout the Tertiary (Madanipour, 2013) and they also cut Quaternary sediments. Since ore-bearing veins formed along the fault zones, it can be speculated that they were active before mineralization and provided suitable pathways for hydrothermal fluid flow. On the other hand, galena deformation at the Zehabad deposit and the Manjil earthquake in 1990 (30 km north of Zehabad) indicate the activity of the faults after mineralization. Therefore, these faults have been considered as premineralization faults, which were reactivated during and after the mineralization.

There are five types of igneous rocks in the area (Figure 2): an Eocene volcanic unit (Annells et al., 1975, 1985; Asiabanha et al., 2009), and four types of late Eocene intrusive rocks (Castro et al., 2013) with compositions of a) monzonite to quartz monzonite (porphyry); b) granite to quartz syenite (granular) not outcropping in the study area, but being observed in drill cores; c) porphyritic microdiorite intrusion; and 4) porphyritic microdiorite dikes. Abundant monzonite enclaves are present in the microdiorite intrusions. All these units have undergone hydrothermal alteration (Figure 3). Castro et al. (2013) suggested a crystallization age of 38.3 ± 0.17 Ma for monzonite to quartz monzonite and granite to quartz syenite, and an age of 37.8 ± 0.28 Ma as the crystallization age of the mafic for the porphyritic microdiorite intrusion and dikes.

The host rocks in the Zehabad area consist of Eocene layered volcanic and volcaniclastic rocks and late Eocene microdiorite porphyry bodies (Figure 4). Lavas are mostly interlayered with tuff units, unlike trachyte to andesite layers in the east of the northern Ghara-Katala that do not contain any tuffaceous interbeds. Eocene tuff and lavas have a compositional range from andesite to rhyolite, among which andesitic rocks are the most widespread host rock in the study area. There are some locally well-bedded interlayers of sandy tuffs and tuffites appearing in green and red.

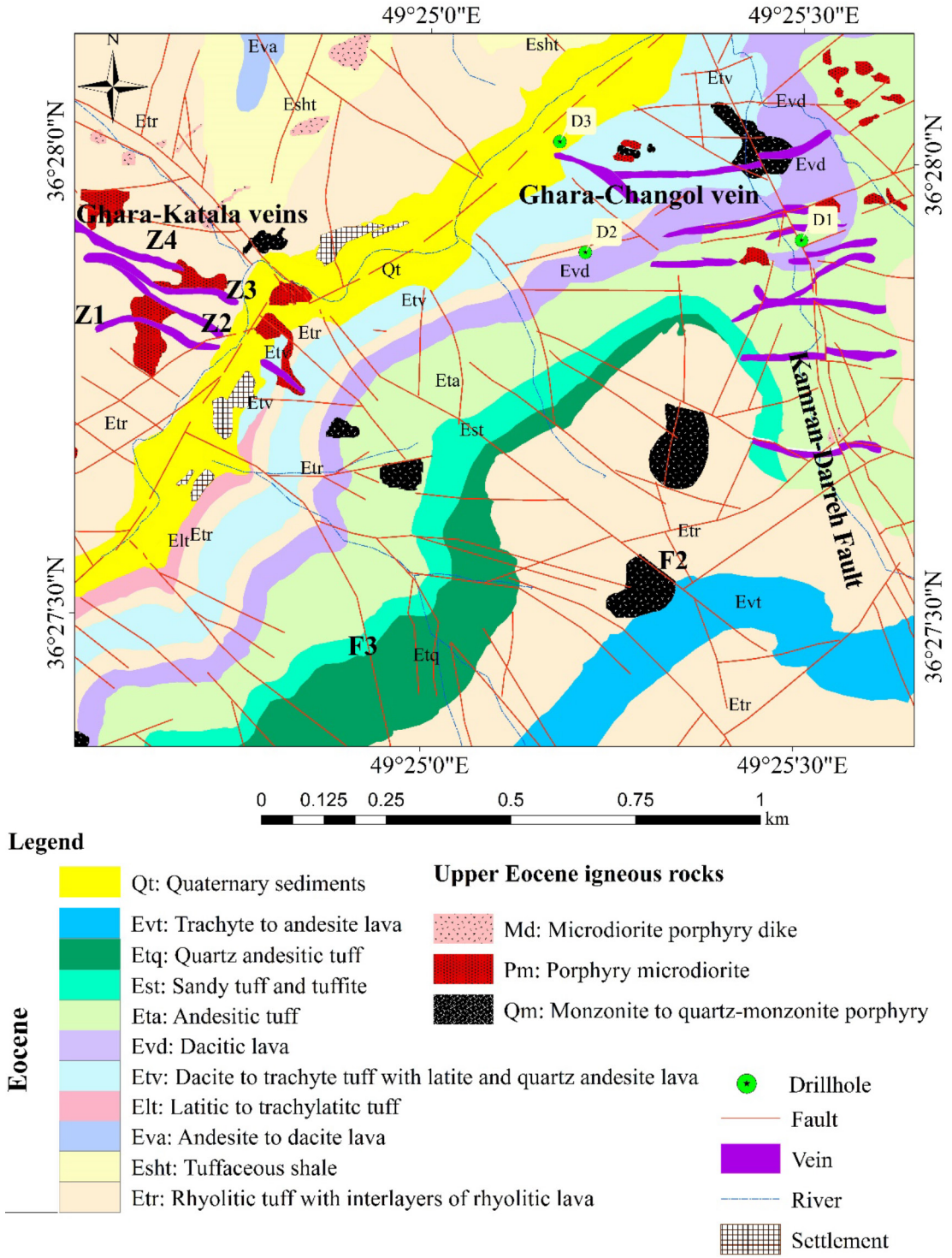

Figure 2. Geological map of the Zehabad deposit.

The volcanic rocks include: I) Porphyritic quartz-andesite that mainly consists of plagioclase, K-feldspar, quartz, and pyroxene, which have been variably altered to quartz, carbonate, sericite, and clay minerals (Figure 5A). II) Dacite that contains plagioclase, K-feldspar, biotite, and pyroxene as phenocrysts and quartz, plagioclase, and K-feldspar as groundmass minerals (Figure 5B). III) Rhyolite with abundant embayed quartz grains, implying primary magmatic source and recrystallization of quartz and feldspar in the matrix. Sodic plagioclase has been

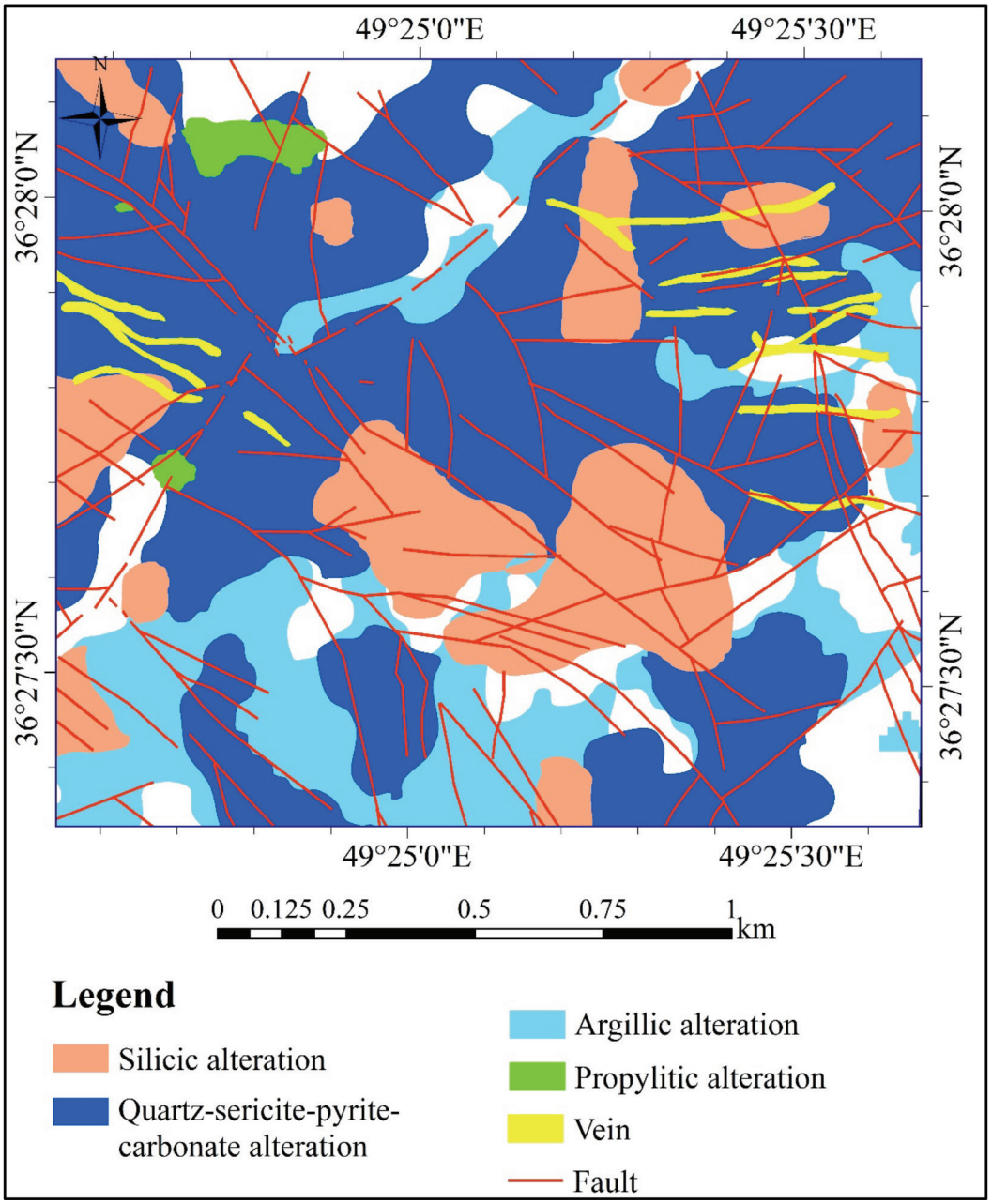

Figure 3. Alteration map of the Zehabad deposit.

carbonatized and sericitized (Figure 5C). Zeolite is abundant around the fault zones. IV) Porphyritic quartz-latite characterized by a fine-grained to microgranular groundmass and phenocrysts that are composed of plagioclase, K-feldspar, and quartz with microlithic texture and ferromagnesian minerals altering to actinolite and chlorite. V) Quartz-trachyte that exhibits a green color that distinguishes this unit from other volcanic rocks. In thin section, K-feldspar and plagioclase show alteration to sericite, calcite, and quartz. A few crystals of biotite and quartz are also seen. The groundmass has trachytic and microlithic textures with porphyritic clasts (Figure 5D).

The volcanoclastic rocks have varying amounts of crystals and lithic fragments, and they can be divided into crystal lithic to lithic crystal tuffs and close to mineralogical veins, which have been brecciated proximal to the veins due to hydrothermal fluid injection. The tuffaceous units include: 1) Rhyolitic tuffs with abundant embayed quartz grains (Figure 5E) that host the southern part of Ghara-Katala veins. 2) Latite to trachy-latite tuffs that contain

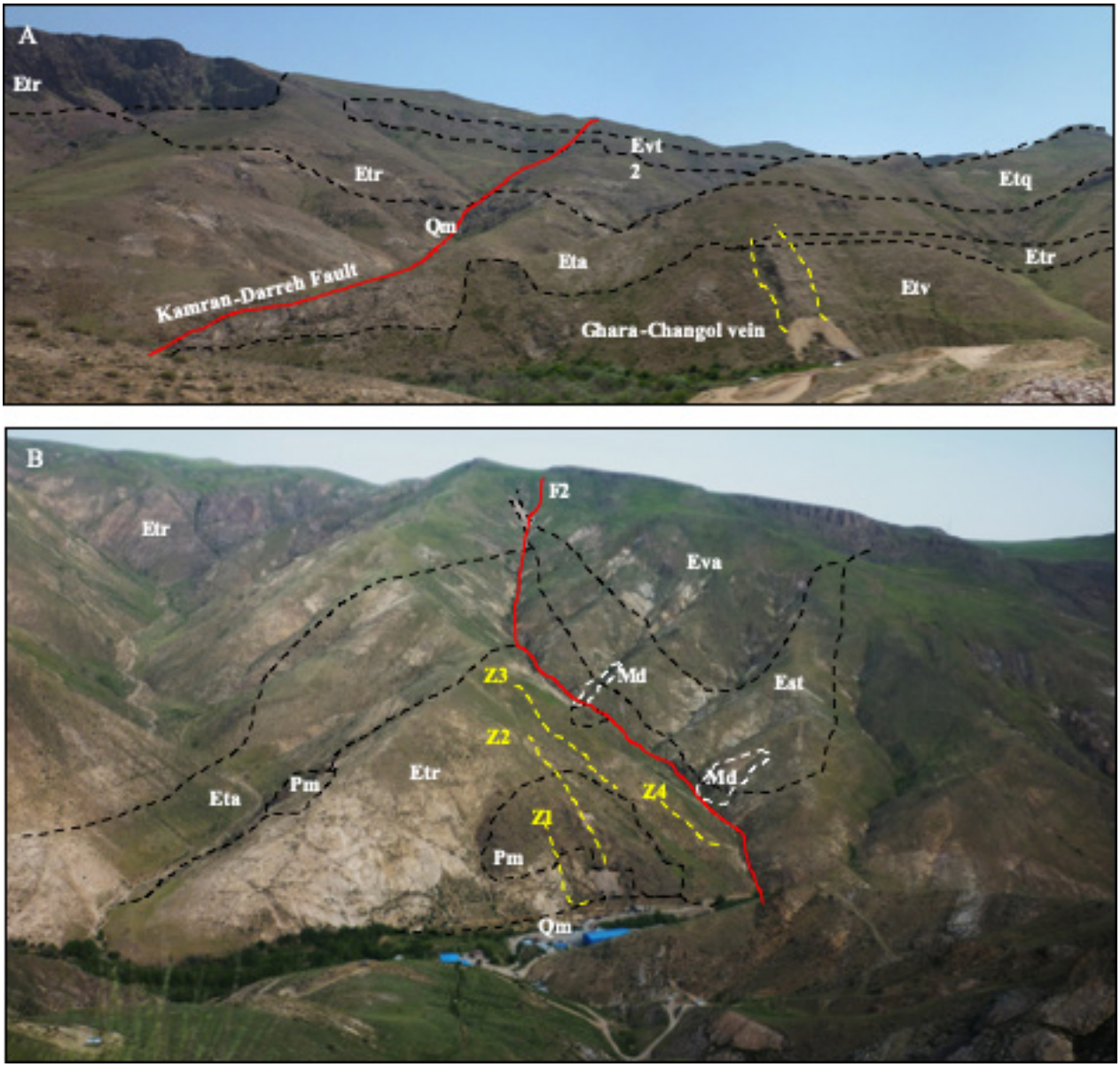

Figure 4. Field photographs of veins and tuffaceous host rocks at the Zehabad deposit: A) Ghara-Changol vein, looking SW; B) Ghara-Katala veins (Z1-Z4), looking NE. Refer to the abbreviations in the legend of Figure 2 for the lithological units.

sector zoned plagioclase (mostly carbonatized) and K-feldspar as major phenocrysts, lesser chlorite, biotite, and rare quartz. These minerals occur in glomeroporphyritic clusters (Figure 5F). Locally, this unit is observed to be interlayered with the dacitic lavas. 3) Minerals observed in the dacitic tuff include embayed quartz, early plagioclase pseudomorphed by calcite and sericite, argillized K-feldspar, and sericitized and chloritized biotite with microgranular porphyritic texture. In trachyte tuff, quartz abundance is less than 5% and has intercalation with the dacitic tuff. 4) The quartz-andesite to andesite unit comprises argillized plagioclase and, in some places, K-feldspar replaced by calcite. Adjacent to mineralizing veins at the Ghara-Changol mine, silicification is widespread.

Porphyritic microdiorite contains sericitized plagioclase with coexisting titanite, K-feldspar, chloritized biotite, chloritized pyroxene as phenocrysts, labradorite, and K-feldspar in the groundmass (Figure 6A). Monzonite to quartz-monzonite porphyry has a light pink to light green color. K-feldspar, plagioclase, and rare pyroxene have been locally altered to chlorite and calcite. In the east of the area, this unit was observed as enclaves in the microdiorite porphyry, which indicates it was emplaced before microdiorite porphyry (Figure 6B). Although granite to

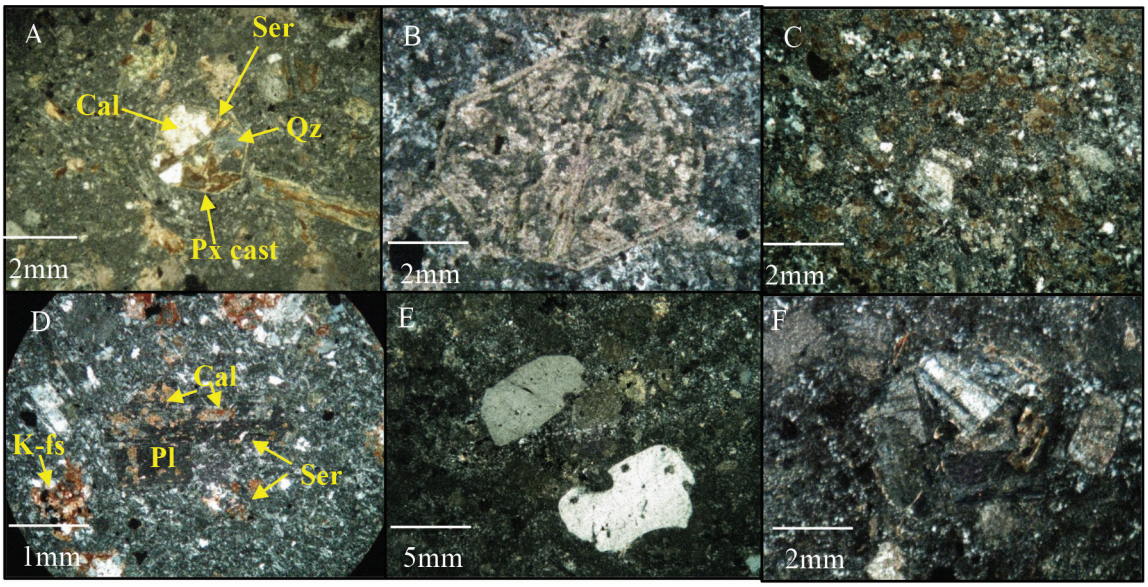

Figure 5. Microphotographs of volcanic rocks in Zehabad deposit. Lavas (A–D) and tuffs (E and F). A) Porphyritic quartz-andesite with pyroxene phenocryst that altered to quartz, carbonate, and sericite. B) Pyroxene phenocrysts in dacite replaced by carbonate and chlorite. C) Rhyolite, showing recrystallization of quartz and K-feldspar in matrix. D) K-feldspar and plagioclase altered to sericite, calcite, and quartz in quartz-trachyte. E) Rhyolitic tuff with embayed quartz crystals. F) Latite to trachy-latite tuff with glomeroporphyritic texture.

quartz-syenite rocks are not exposed in the surface, they were observed in the drill core with up to 10-m-thick leucocratic bodies and have a light pink color. This unit is composed of mostly quartz and K-feldspar with graphitic texture (Figure 6C). Microdiorite porphyry dike (and sill) outcrops are dispersed in the region, but several outcrops were observed near the Ghara-Katala veins (Figure 2). The resemblance of the mineralogical composition and the proximity to the microdiorite porphyry intrusions suggest a genetic relationship between the units. In thin sections, microlithic porphyry texture with pyroxene, amphibole (hornblende), and plagioclase phenocrysts are visible as well as flow microlithic, ophitic, intersertal, and glomeroporphyry textures (Figure 6D).

4. Mineralized veins

Economic and actively mined ore-bearing breccia veins occur parallel to 80–130° trending fractures and faults. Based on recent studies (Shahbazi and Ghaderi, 2014; Shahbazi et al., 2018) and field observation at the Zehabad deposit, these breccia veins seem to have formed along with microdiorite and tuff contacts and occur in the form of veins within hydrothermal breccia zones.

4.1. Characteristics of mineralized veins

At the Zehabad deposit, two out of 30 known veins are currently under exploitation. The first vein system, the Ghara-Changol vein, with a 125° trend and vertical dip, has a strike length of about 550 m, and its thickness varies from 0.3 to 2 m (Figures 2, 4A, and 7A). The second vein system, Ghara-Katala, is composed of four subvertical veins striking 80–120° with a strike length of 260–300 m at the surface (Figure 7B). The vertical Z1 vein has 200 m strike and a 80–110° trend. Z2 is the largest and the only actively mined vein in this series, with 450 m strike, 120° trend, and vertical dip. Z3 has 250 m strike, 80–120° strike, and vertical dip, and finally, Z4 has 130 m strike with 110° strike and vertical dip (Figure 7B). All these veins are located in the silicic breccia zone.

The breccia zones consist of angular to subrounded fragments (0.1 to 20 cm in size) composed of silicified and argillized rhyolitic to dacitic tuffs in a matrix of quartz-base metal sulfides (Figure 7C) that are crosscut by late-stage vuggy, comb-textured barren quartz veinlets (Figure 7D). Within the mineralized zone, the host rocks are intensely silicified and contain patchy stockworks of quartz-base metal sulfide veinlets with drusy texture.

4.2. Mineralization stages and ore mineralogy

Five discrete stages of mineralization were identified at the Zehabad deposit based on ore mineralogy, structure, and ore textures.

The main ore minerals at Zehabad include pyrite, chalcopyrite, bornite, sphalerite, galena, and sulfosalts, especially tennantite-tetrahedrite, which occur as vein and veinlets, disseminations, exsolution, replacement, and massive accumulations in veins and breccia matrix. The paragenetic sequence is shown in Figure 8.

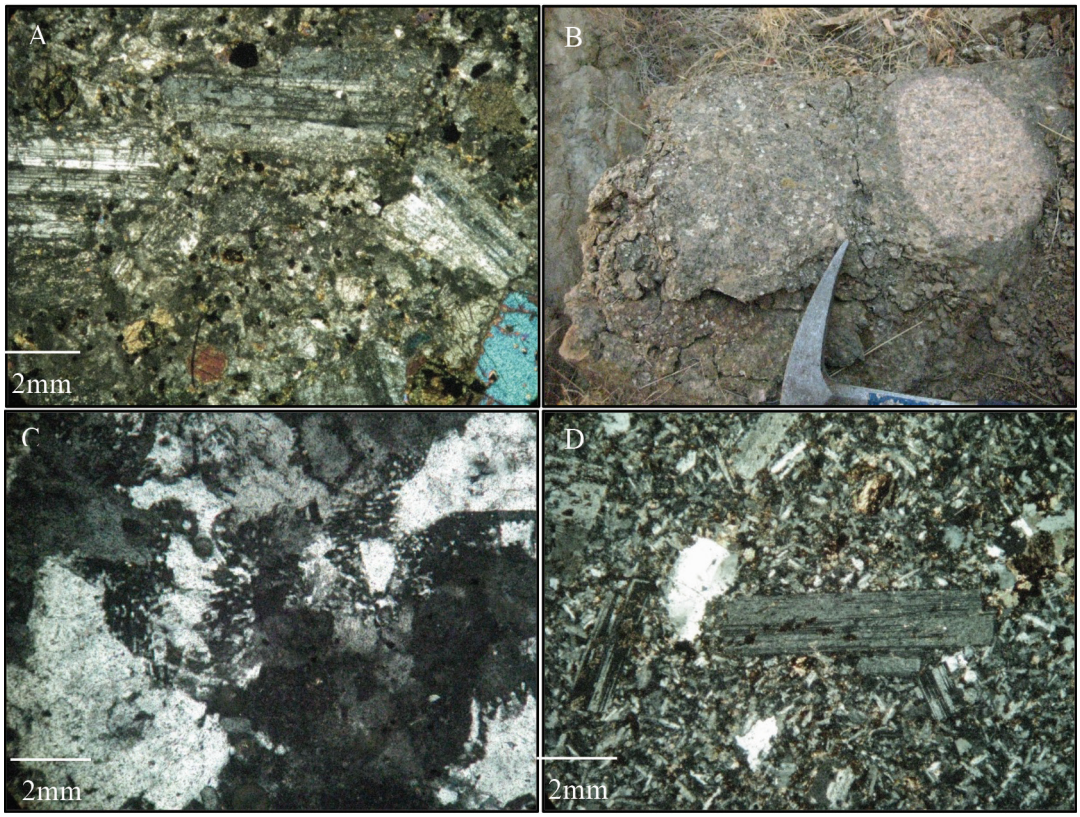

Figure 6. Photographs of igneous rocks at Zehabad deposit. A) Microphotograph showing porphyritic microdiorite with sericitized plagioclase and pyroxene phenocrysts. B) Enclave of monzonite to quartz-monzonite porphyry in microdiorite. C) Granite with graphic texture. D) Microdiorite porphyry dike showing porphyritic texture with plagioclase and quartz phenocrysts surrounded by plagioclase microliths.

The first stage is characterized by disseminated framboidal pyrite intergrown with sphalerite and minor chalcopyrite (Figure 9A). Due to the introduction of subsequent phases of fluid, these sulfide minerals remain as disperse patches in chalcopyrite from the following stage (Figure 9A). The second stage is represented by coarse-grained euhedral sulfide-bearing quartz veins of between 0.1 mm and 5 cm. These veins mostly contain chalcopyrite, bornite, and pyrite, as well as sphalerite and sulfosalts (Figures 9B and 9C), which have been cut by specular hematite and replaced by stage 4 ores. Sulfosalt minerals are very fine-grained for accurate identification without using other analytical tools (e.g., electron probe microanalysis).

At stage 2, pyrite occurs as euhedral to subhedral disseminated crystals (<0.2 to 5 mm in size), or massive aggregates in veins. This pyrite is coeval with subhedral to anhedral chalcopyrite (Figure 9B), bornite, and sphalerite. Chalcopyrite usually occurs at stage 2, replacing the framboidal sulfides of stage 1 along boundaries and fractures in the main part of the ore zones. In some samples, chalcopyrite can be seen as inclusions in sphalerite. Small amounts of bornite were observed in the quartz veins, where it usually occurs in margins and fractures of chalcopyrite and was formed simultaneously with to immediately after chalcopyrite (Figure 9C).

Sphalerite occurs as optically clear, honey-colored to light brown and green (Fe-poor) variety, typically forming massive, coarse (generally about 5 mm in size) subhedral to anhedral grains. Sphalerite postdates chalcopyrite, but in some cases, both minerals appear to have coprecipitated because they show equilibrium intergrowths (Figure 9B). In some samples, chalcopyrite is distributed randomly in sphalerite, so it can be concluded that these minerals coprecipitated (Bortnikov et al., 1991).

In the third stage, due to the hydrothermal ore-bearing fluid reintroduction, the host rock underwent brecciation and earlier fractures reopened. Along with this, specular hematite, native gold, chalcedony, and bladed calcite were deposited in veins (Figures 9D and 9E). At this stage, the first phase of gold mineralization occurs together with specular hematite and bladed calcite or as inclusions in quartz (Figures 10A–10D).

The fourth stage is the most abundant, widespread, and economically important ore-forming stage at Zehabad and

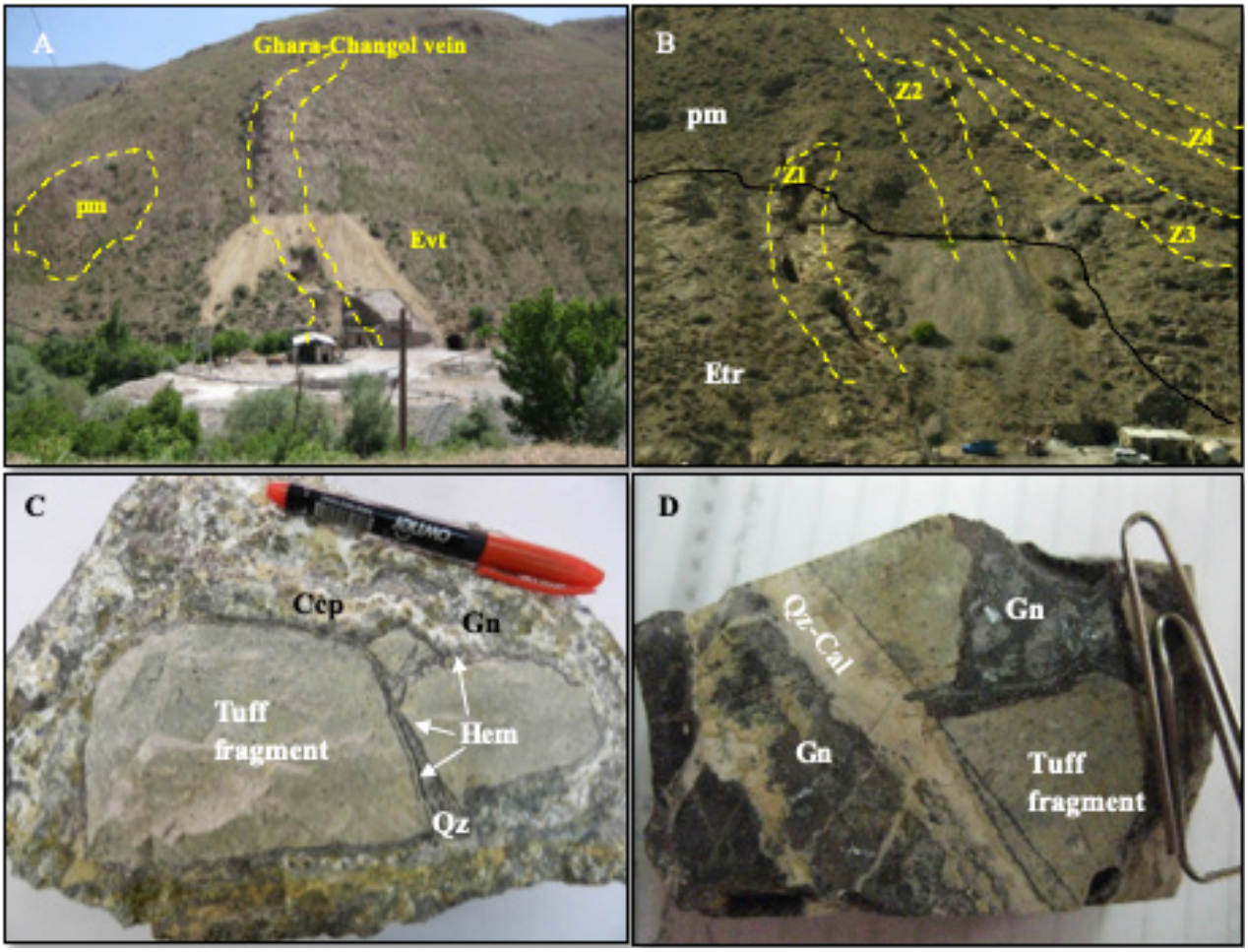

Figure 7. A) Outcrop of Ghara-Changol vein; B) outcrop of the four Ghara-Katala veins; C) cockade texture characterized by tuffaceous breccia clasts cemented by hydrothermal minerals (quartz and sulfides); D) quartz-carbonate vein that crosscut the mineralized zone. Hem: hematite, Ccp: chalcopyrite, Gn: galena, Qz: quartz, Cal: calcite.

is represented by veins consisting of central quartz (<1 cm to 2 m width) and marginal breccia zones (0.5 cm to 1 m width) containing variable amounts of galena, sphalerite, tennantite-tetrahedrite, pyrite, native gold (Figures 9F–9H and Figures 10E and 10F) and other sulfosalts. Sphalerite is widespread in stage 4 veins and breccias (Figure 9F), but it has equilibrium boundaries with galena and has replaced chalcopyrite. Inclusions of gold were observed within sphalerite in a sample collected from the Ghara-Changol mine (Figure 10E). Galena occurs as coarse euhedral to subhedral grains of up to 1 cm size. It usually replaces chalcopyrite (Figure 9F). Galena was mostly intergrown with sphalerite, but in some cases, galena veinlets crosscut sphalerite (Figures 9G and 9H). Gold inclusions occasionally occur within galena (Figure 10F). Tennantite-tetrahedrite occurs within stage 4 veins and in breccia matrix, forming grains of <5 mm. Tennantite-tetrahedrite replaces chalcopyrite along grain margins and fractures, indicating that it is late in the ore paragenesis. These solid-solution minerals coprecipitated with galena and sphalerite (Figure 9F). Pyrite in stage 4 replaced bladed calcite and so formed as bladed crystals (Figures 9I and 9J).

The fifth and last stage of hydrothermal activity is represented by barren quartz-calcite veins with thicknesses reaching up to 30 cm. In this stage, galena, sphalerite, and chalcopyrite that formed in previous stages were broken, fragmented, and incorporated in stage 5 veins with quartz-calcite cement (Figures 9K and 9L). Quartz typically occurs as coarse-grained euhedral crystals of up to 2 cm in length in filling vugs and showing comb texture.

Chalcocite, covellite, digenite, gypsum, smithsonite, cerussite, malachite, azurite, iron oxy-hydroxides, jarosite, and clay minerals formed during the supergene stage.

5. Hydrothermal alteration

Silicification developed in association with 4 out of 5 mineralization stages, and it is the main alteration type

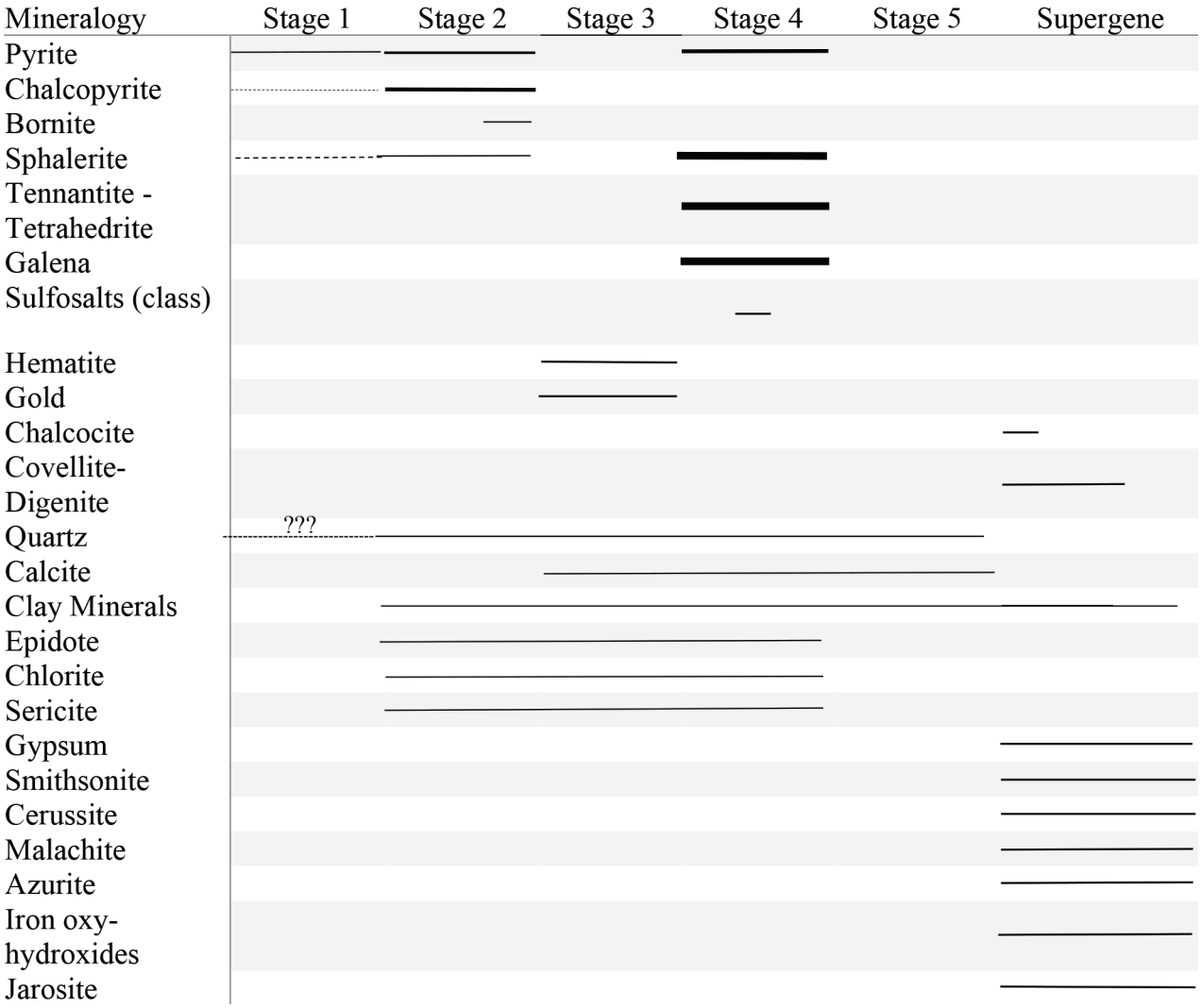

Figure 8. Paragenetic sequence of ore and gangue minerals from the Zehabad deposit.

related to Zehabad mineralization, represented as: 1) coarse-grained quartz (up to 3 cm) with chalcopyrite and minor pyrite mineralization (Figure 11A); 2) chalcedony with hematite and gold mineralization (Figure 11B); 3) relatively fine-grained quartz (<1 cm) with pyrite, galena, sphalerite, tennantite-tetrahedrite, and gold mineralization (Figure 11B); and 4) coarse-grained quartz (up to 2 cm in size) veins without any sulfide minerals (Figure 11C).

The most important quartz textures in stage 1 include mosaic and comb textures (Figures 12A and 12B), and in stage 2 fibrous chalcedony as shown in Figure 8D. In stages 3 and 4, quartz occurs in crustiform, comb, and cockade forms (Figures 12B–12D). Widespread sericite (illite and rare fine-grained muscovite), quartz-pyrite, and carbonate alteration (Figure 13A) formed adjacent to the mineralized veins and were deposited contemporaneously with ore-bearing quartz-sulfide, barren thick quartz veins, and silicification.

Argillic alteration containing kaolinite and montmorillonite covers most outcrops of the area, developed in wall-rocks, and is associated and synchronous with silicification and sericite-quartz-pyrite-carbonate alteration. These minerals were also encountered at deeper levels in the drill core (down to 200 m), suggesting that they are hypogene in origin. In thin sections, feldspars and biotite have been replaced by kaolinite and montmorillonite minerals (Figure 13B).

Propylitic alteration occurs distally to the mineralized veins. This alteration affected the microdiorite and andesite, and it is characterized by replacement of primary igneous minerals such as plagioclase, pyroxene, and amphibole by epidote, calcite, chlorite, and sericite (Figure 13C).

Carbonatization is the late stage of alteration, characterized mainly by calcite and less commonly by rhodochrosite and quartz veins as well as clay minerals

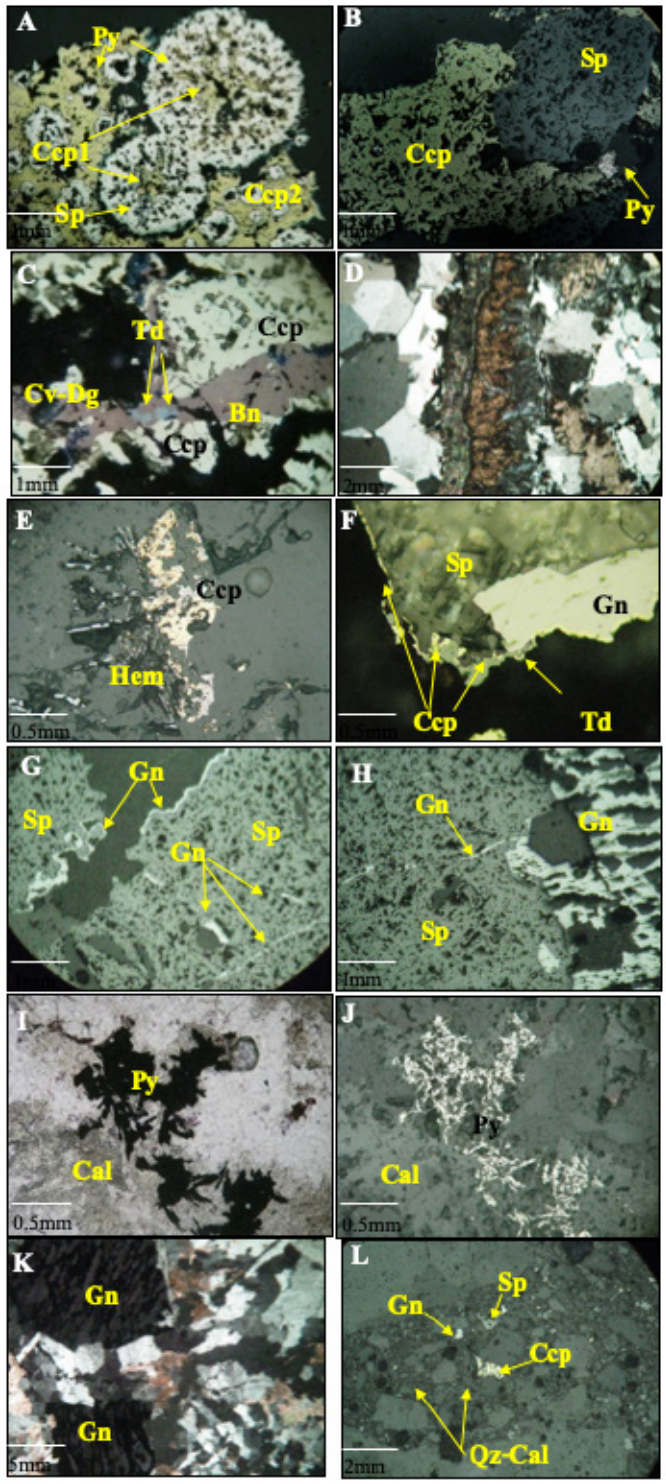

Figure 9. A) First-stage framboidal sulfides (especially pyrite) surrounded by stage 2 chalcopyrite. B) Pyrite, chalcopyrite, and sphalerite from stage 2 mineralization. C) Tetrahedrite replacing bornite intergrown with chalcopyrite. D) Specular hematite, chalcedony, and bladed calcite from stage 3 mineralization. E) Chalcopyrite being overgrown by specular hematite in stage 3. F) Replacement of chalcopyrite by galena, sphalerite, and tennantite-tetrahedrite in stage 4 mineralization. G and H) Galena veinlets cross-cutting sphalerite II. I and J) Replacement of bladed calcite by pyrite in stage 4. K) Late-stage quartz-carbonate vein cross-cutting galena. L) Fragments of sulfide minerals in matrix of quartz and calcite in stage 5. Ccp: chalcopyrite, Bn: bornite, Cv-Dig: covellite-digenite, Sph: sphalerite, Py: pyrite, Cal: calcite, Td: tennantite-tetrahedrite; Gn: galena. D and I in transmitted light. Other photos in reflected light.

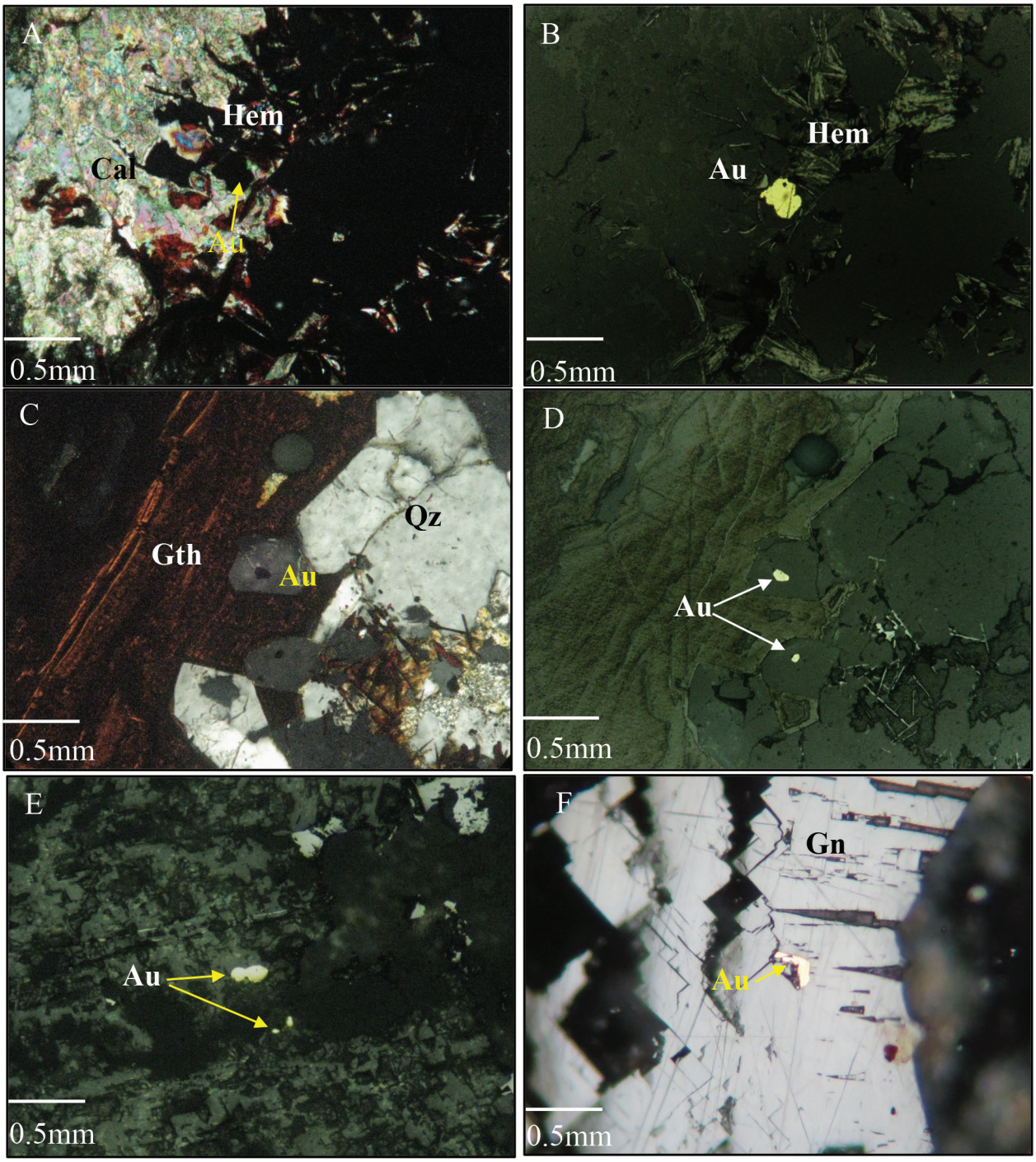

Figure 10. A) Gold mineralization associated with bladed calcite in stage 3 (in XPL). B) Gold mineralization associated with specular hematite in stage 3 (in reflected light). C and D) Gold inclusions in quartz from stage 3 mineralization (C: in PPL, D: in reflected light). E) Gold inclusion in sphalerite in stage 4 mineralization. F) Gold inclusion in galena in stage 4 mineralization. Cal: calcite, Hem: hematite, Au: gold grain. Gth: goethite, Qz: quartz, Sph: sphalerite, Gn: galena.

associated with minor calcite in the breccia matrix. It is clear that the calcite veins are the latest hydrothermal alteration (Figure 14).

6. Sulfur isotopes

The $\delta^{34}S$ values from sphalerite (with no chalcopyrite inclusions) at the Zehabad veins in mineralization stage

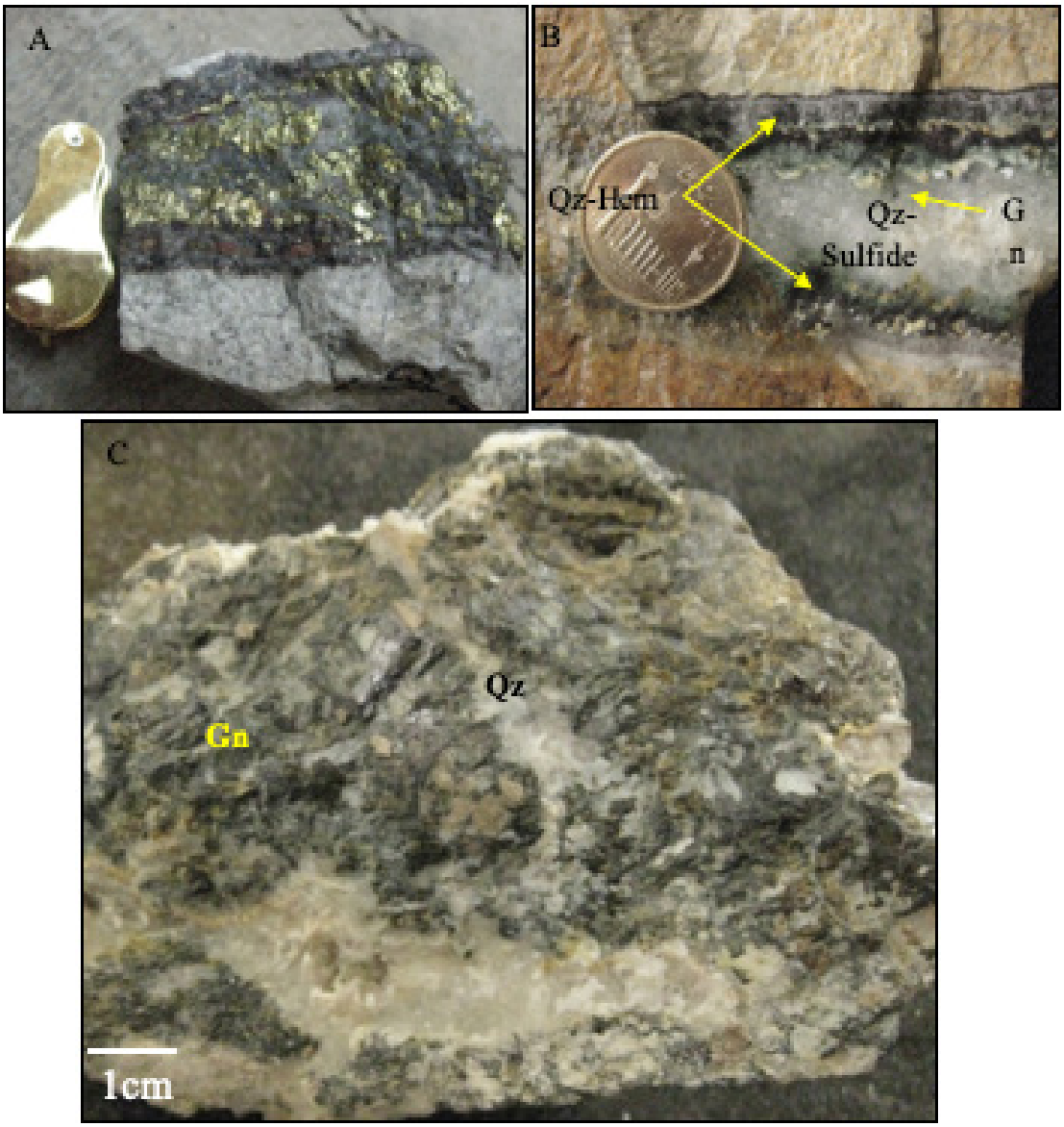

Figure 11. A) Quartz veins with chalcopyrite mineralization (stage 2). B) Quartz-hematite deposited in stage 3. Later reopening of the vein resulted in stage 4 quartz-sulfide precipitation. C) Coarse-grained stage 4 quartz vein cross-cutting galena. Qz: quartz, Hem: hematite, Gn: galena.

3 range from –7.6‰ to –0.8 ‰, (avg. = –5.0 ± 1.7‰, n = 13) and $\delta^{34}S$ values of galena from the same stage range from –10.1‰ to –5.2‰ (avg. = –8.3 ± 1.7‰, n = 7). The $\delta^{34}S$ composition of chalcopyrite from stage 2 ranges from –8.3‰ to –4.7‰ (avg. = –6.2 ± 1.4‰, n = 6) and one covellite sample from the same stage has a $\delta^{34}S$ composition of –0.9‰ (Table; Figure 15). At the Zehabad deposit, $\delta^{34}S$ values increase in the order of galena < sphalerite, as is expected under equilibrium conditions (Ohmoto and Rye, 1979). However, since chalcopyrite formed in stage 2 and galena and sphalerite were deposited in stage 4, chalcopyrite cannot fit in the above range.

7. Discussion

7.1. Sources of sulfur

The homogeneous values of $\delta^{34}S$ in the Zehabad deposit suggest that the sulfur in all analyzed samples was derived from a common source. As mentioned above, there are no hypogene sulfate minerals in the veins, suggesting that sulfur was transported in a reduced state. All of the $\delta^{34}S$ values are negative, with an average of about –5.8 ± 2.35‰ (n = 27). According to Hoefs (2009), negative $\delta^{34}S$ values do not necessarily rule out a direct magmatic source. Magmatic fluids are the dominant fluids in most IS and HS epithermal deposits (Corbett and Leach, 1998;

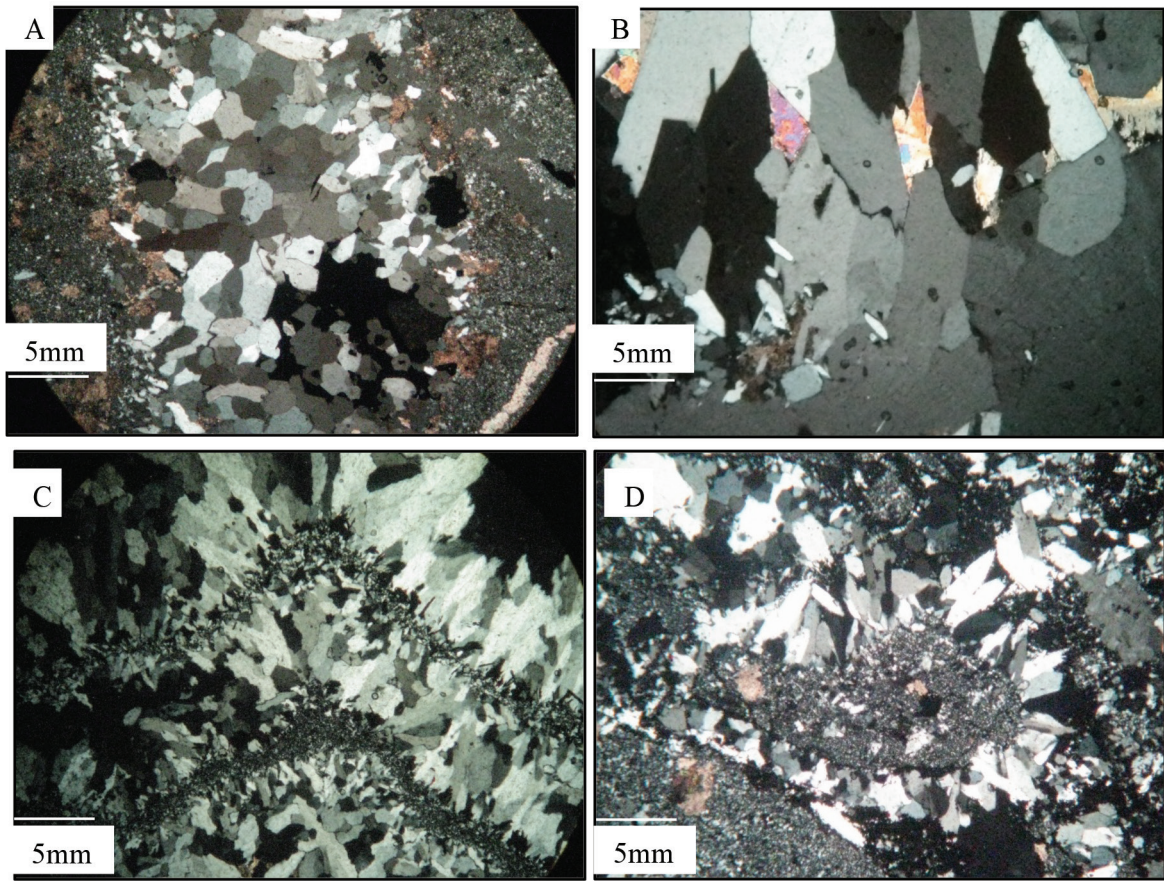

Figure 12. Different textures of ore-bearing quartz veins in stage 4: A) mosaic, B) comb, C) crustiform, D) cockade.

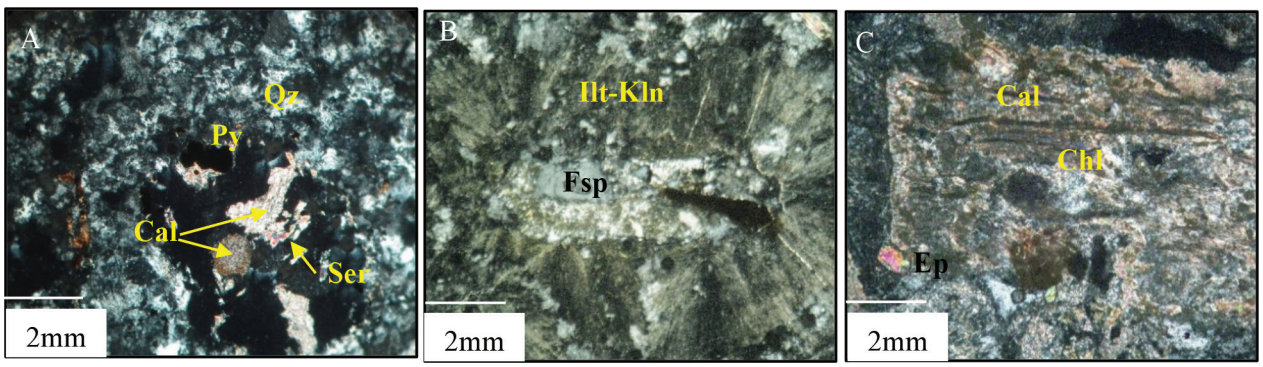

Figure 13. Microphotographs showing various alteration types. A) Phyllic alteration in quartz monzonite including quartz, sericite, calcite, and pyrite. B) Argillic alteration in tuff showing feldspar being replaced by clay minerals such as illite and kaolinite. C) Propylitic alteration in andesitic tuff, plagioclase altered to chlorite, epidote, and calcite. Fsp: feldspar, Ilt: illite, Kln: kaolinite, Cal: calcite, Chl: chlorite, Ep: epidote, Qz: quartz, Py: pyrite, Ser: sericite.

Hedenquist et al., 2000; Sillitoe and Hedenquist, 2003). There are no sedimentary rocks at the Zehabad deposit and its surroundings that could act as a depleted ^{34}S source. The sulfur isotopic compositions of sulfides are functions of temperature, pH, and fO_2 of the solution during deposition (Ohmoto, 1972), and negative $\delta^{34}S$ values may be indicative of a magmatic source as observed in other districts (Field and Fifarek, 1985; Seal and Rye, 1992; Rye, 1993; Sherlock et al., 1995). Here, we propose that sulfur in the mineralized veins was probably derived from the contemporaneous magmatic activity or through leaching of the older volcanic rocks, similar to Sechangi

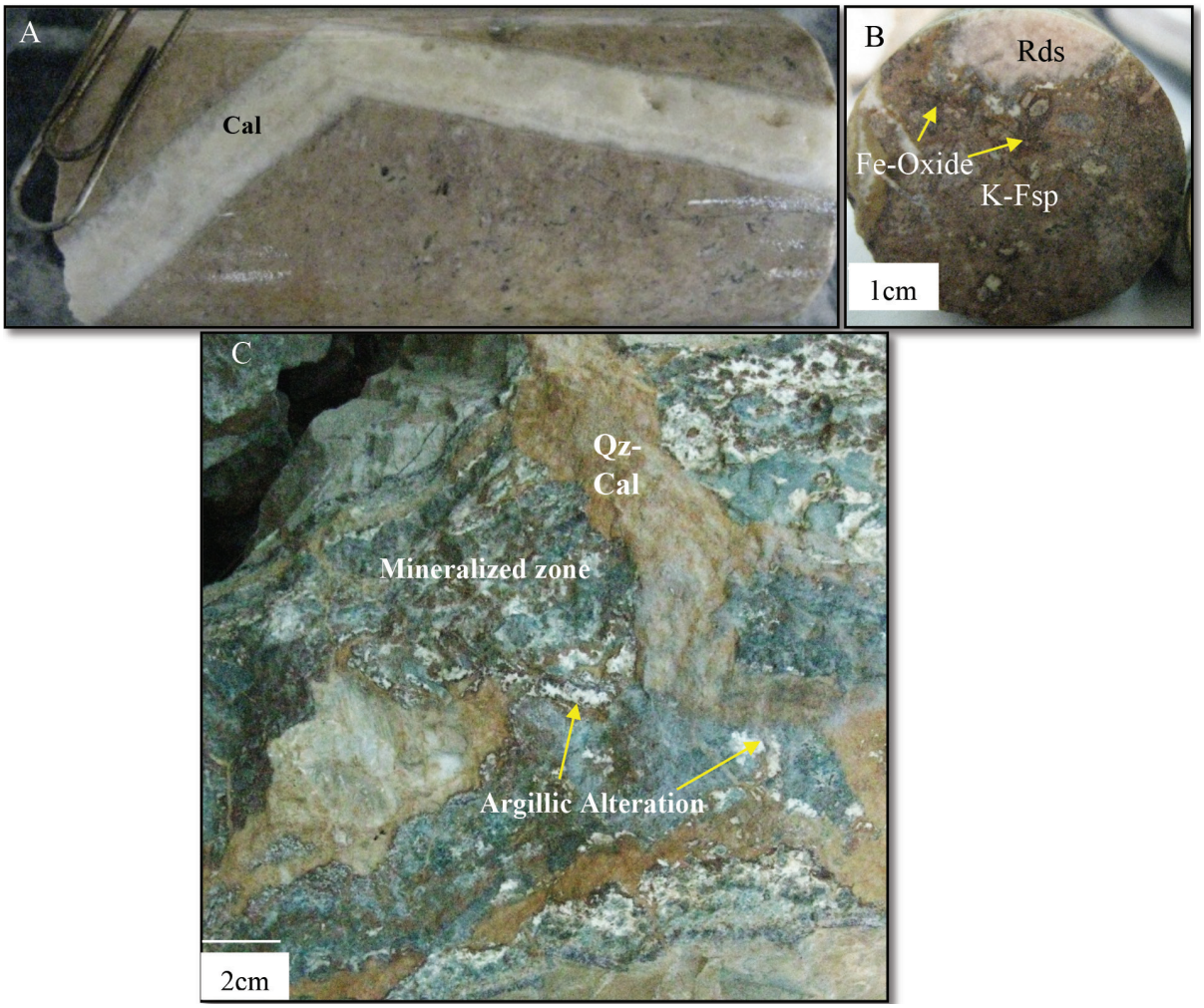

Figure 14. Carbonatization: A) calcite vein in andesitic tuff; B) open space filling texture of rhodochrosite; C) early lead-zinc mineralization cross-cut and brecciated by quartz-calcite vein in argillized dacitic tuff. Cal: calcite, Qz: quartz, K-Fsp: K-feldspar, Rds: rhodochrosite.

(Malekzadeh-Shafaroudi and Karimpour, 2015) and to the Goloujeh district of NW Iran (Mehrabi et al., 2016). The light sulfur isotope values could be the result of changes in the oxidation state due to hydrothermal fluid boiling and selective oxidation of $H_2{}^{34}S$, as observed in Valles Caldera (McKibben and Eldridge, 1990), the Fakos Peninsula (Fornadel et al., 2012), and Kuh-Pang (Rajabpour et al., 2017). Deposition of specular hematite in quartz veins and bladed calcite (now replaced by pyrite), simultaneous with chalcopyrite mineralization, can be taken as evidence of the role of boiling in the formation of this deposit (Simmons and Christenson, 1994; Hedenquist et al., 2000; Leach and Corbett, 2008; Hanilçi et al., 2015; Wang et al., 2019). On the other hand, Leach and Corbett (2008) pointed out that the formation of some minerals such as hematite, kaolinite, and carbonates may suggest the mixing of magmatic-sourced fluids with oxidized meteoric waters.

7.2. Sulfur isotope geothermometry

Three sphalerite-galena pairs (from stage 4), showing three different types of textural relationships, were analyzed to determine equilibrium isotope temperatures. Sample Qo5 from the banded ore, sample L5-2 from the brecciated ore where clasts of sulfide ore minerals are cemented by quartz, and sample L8-3-2 from the massive ore were analyzed. Mineral pairs in all samples show equilibrium boundaries under the microscope. The sphalerite-galena pairs from Zehabad, using the equations from Ohmoto and Rye (1979), yielded temperatures from 276 to 288 ± 20 °C, which fall within the typical formation temperatures of IS epithermal deposits (Sillitoe and Hedenquist, 2003).

7.3. Ore deposition processes and mineralization type

Upon brecciation and fracturing, hydrothermal fluids may undergo boiling due to sudden pressure drop; gaseous

Table. The $\delta^{34}S$ values for sulfide samples from the Zehabad deposit.

Sample	**Average fluid temperature**	Chalcopyrite	Sphalerite	Galena	**1000 ln α**	**Hydrothermal fluid (‰, CDT)**
K6	207		-6.3		0.4	**-6.7**
K13b	207		-0.8		0.4	**-1.2**
K13g	207		-3.1		0.4	**-3.5**
K18	207			-7.7	-2.8	**-4.9**
Qo5	229		-5.1		0.4	**-5.5**
Qo5	229			-6.9	-2.5	**-4.4**
Qo10	229	-4.7			0.2	**-4.9**
Qo18	229		-4.5		0.4	**-4.9**
L5-2	226			-10.0	-2.6	**-7.4**
L5-2	226		-7.6		0.4	**-8.0**
L6-3	226		-6.2		0.4	**-6.6**
L6-5	226			-10.1	-2.6	**-7.5**
L8-1-1	226			-9.4	-2.6	**-6.8**
L8-3-1	226	-8.3			0.2	**-8.5**
L8-3-2	226			-8.6	-2.6	**-6.0**
L8-3-2	226		-6.3		0.4	**-6.7**
L8-3-6	226		-6.1		0.4	**-6.5**
L8-3-6	226	-6.7			0.2	**-6.9**
L8-3-7	226	-4.8			0.2	**-5.0**
L8-3-7	226		-3.2		0.4	**-3.6**
L9-1	226	-6.3			0.2	**-6.5**
L9-1	226		-5.3		0.4	**-5.7**
L9-2	226		-5.0		0.4	**-5.4**
L9-4	226			-5.2	-2.6	**-2.6**
						-5.3

phases such as CO_2 and H_2S leave the system, leading to precipitation of chalcedony, bladed calcite, and gold (Buchanan, 1981; Henley, 1984; Hedenquist et al., 2000; Poliquin, 2004; Gülyuz et al., 2018). Gold precipitation occurs at this stage, and then the fO_2 decreases and sulfide minerals form as fracture fillings. It seems that bladed crystals of pyrite fill the bladed calcite casts by replacing them and depositing immediately after boiling.

According to Sillitoe and Hedenquist (2003), based on the sulfidation state of the hypogene sulfide assemblages, epithermal deposits are divided into three types: high sulfidation (HS), intermediate sulfidation (IS), and low sulfidation (LS).

The Zehabad deposit could be regarded as an IS epithermal mineralization. Intermediate-sulfidation epithermal deposits occur in neutral stress to mildly extensional arc and compressive back-arc settings during arc volcanism (Sillitoe and Hedenquist, 2003). These deposits contain chalcopyrite, tetrahedrite-tennantite (which form from IS-state liquid; Einaudi et al., 2003; Sillitoe and Hedenquist, 2003), and Fe-poor sphalerite, dominantly formed by magmatic fluids (Einaudi et al., 2003). Quartz and illite are the major alteration and gangue minerals (Wang et al., 2019). Intermediate-sulfidation epithermal deposits contain more abundant base-metal sulfides and illite.

Recently, Wang et al. (2019) described the characteristics of IS deposits in more detail. They suggested that IS deposits form from the mixing of magmatic and meteoric fluids in andesitic rocks that may be cogenetic with deeper porphyry-related intrusions. The presence of Fe-poor sphalerite indicates relatively lower oxidation states of ore-bearing fluids, while sphalerites in HS epithermal deposits are Fe-rich. One of the most important differences between

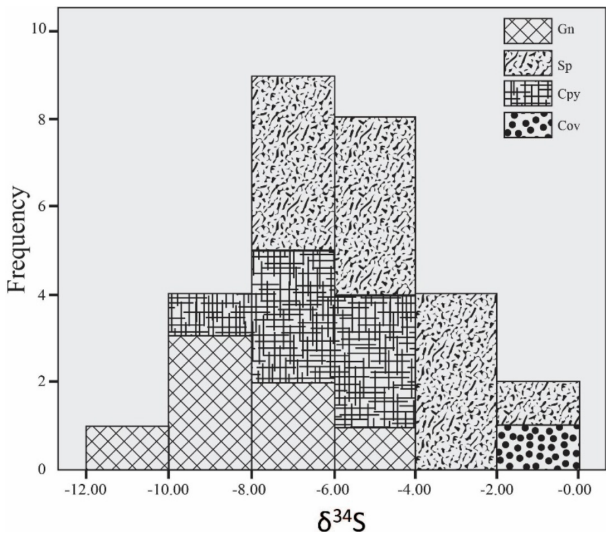

Figure 15. Histogram showing range of $\delta^{34}S$ values from sulfide minerals from different stages of mineralization at the Zehabad deposit.

IS epithermal deposits when compared with HS and LS deposits is the predominance of Mn-carbonate (and silicate) gangue such as rhodochrosite and widespread illite alteration.

Intermediate-sulfidation epithermal deposits usually occur in association with calc-alkaline volcano-plutonic complexes in magmatic arcs (Sillitoe, 2010), but some intermediate-sulfidation deposits also occur in back-arc (e.g., Çöpler deposit; Imer et al., 2013, 2016), or collisional or postsubduction tectonic settings (e.g., Roşia Montană; Heinrich and Neubauer, 2002; Richards, 2009; Wang et al., 2019). These deposits form in <1 km depth, contain Zn-Pb-Cu-Ag±Au, and may be located alongside porphyry Cu-Au deposits (Imer et al., 2013, 2016; Sillitoe et al., 2013).

Zehabad possesses characteristics of most IS epithermal deposits, as described in detail by various researchers (Hedenquist et al., 2000; Sillitoe and Hedenquist, 2003; Wang et al., 2019). This is evidenced by: 1) index epithermal textures such as hydrothermal veins and breccias with vug infill, comb, banding, crustiform, and cockade textures; 2) hydrothermal alteration represented by sericite-quartz-pyrite-carbonate; 3) relatively high base metal (e.g., Cu, Pb, and Zn) abundance; 4) ore assemblage characterized by chalcopyrite, Fe-poor sphalerite, galena, gold, tennantite-tetrahedrite, and other sulfosalts; 5) range of sulfur isotope compositions between –0.8‰ and –10.1‰ (avg. –5.8‰) showing a possible magmatic source for ore-bearing hydrothermal fluids; 6) relatively high temperature range of 276–288 ± 20 °C hydrothermal fluids; and 7) presence of shallow-level intrusive bodies adjacent to ore-bearing veins.

The galena-sphalerite pair minerals yielded a temperature of mineralization in the range of 275–285 °C, which is typical of epithermal type deposits (e.g., Yilmaz et al., 2007, 2010; Kouhestani et al., 2012, 2015; Mohammadi-Niaei et al., 2015). The distribution of silicification together with mineralization, the sericite-quartz-pyrite-carbonate zone close to the veins, and the propylitic zone away from the veins are consistent with the characteristics of IS epithermal deposits.

The distribution pattern of hydrothermal alteration at the Zehabad deposit is indicative of epithermal features, and alteration minerals indicate the near-neutral to mildly acidic pH conditions for ore fluids. According to microscopic and field studies, there are quartz, kaolinite, locally dickite, smectite, siderite, illite, carbonate (dominated by calcite and minor rhodochrosite), and chalcedony as alteration minerals at the Zehabad deposit that are an index of slightly acidic conditions with temperatures in the range of 180–310 °C (Henley and Ellis, 1983; Reyes, 1990; Thompson and Thompson, 1998) and magmatic source (Simmons and Browne, 2000; Wang et al., 2019). Widespread illite alteration shows the less acidic nature of fluids. Based on Corbett and Leach (1998), the pH of the argillic alteration is in the range of 4–6, while phyllic (illite/muscovite-quartz-pyrite + anhydrite + carbonate) alteration forms in the pH range of 5–6, implying weakly acidic fluids.

According to Wang et al. (2019), major gangue minerals in IS epithermal deposits are quartz, illite, and carbonate, particularly Mn-carbonate, and the presence of base metal sulfides suggests that the ore-forming fluids probably have salinities between 1 and 10 wt.% NaCl equiv. At the Zehabad deposit, the abundance of galena and sphalerite implies that the fluids were probably saline, because base metals can only be efficiently transported by chloride complexes. In addition, the sulfur isotope results are in accordance with a magmatic source for sulfur.

8. Conclusions

The Zehabad deposit occurred in the Eocene volcanic rocks of NW Iran. Late Eocene intrusive bodies in this area that belong to the Arasbaran-Tarom high potassium calc-alkaline batholith have similar petrographic and geochemical characteristics as well as geodynamic positions. Arasbaran-Tarom shows arc magmatism signatures. The deposit contains chalcopyrite, galena, Fe-poor sphalerite, tennantite-tetrahedrite, pyrite, sulfosalts, and gold minerals. Arsenopyrite and pyrrhotite were not observed at the deposit. Quartz, kaolinite, dickite, smectite, siderite, illite, calcite (and minor rhodochrosite), and chalcedony are the most important gangue minerals. There are no alunite and adularia as alteration or mineralization products in the

area, but illite has a widespread presence. Mineralization is accompanied by silicification. Bladed calcite and banding textures imply that the Zehabad deposit formed from boiling. The range of sulfur isotope data from the separated minerals (chalcopyrite, sphalerite, and galena) occurs within –0.8‰ to –10.1‰. Our study shows that the sphalerite-galena pairs formed at 276–288 °C. We suggest that the Zehabad deposit is the largest discovered intermediate-sulfidation base and precious metal epithermal deposit in the western Alborz-Azerbaijan structural zone of NW Iran.

Acknowledgments

This paper was a part of the first author's PhD thesis at Tarbiat Modares University, Tehran, Iran. We would like to thank the Iranian Mines and Mining Industries Development and Renovation Organization (IMIDRO) for financial support. Hossein Kouhestani provided helpful comments on an earlier version of the manuscript. We would like to acknowledge Panagiotis Voudouris and two anonymous reviewers for their constructive reviews of the manuscript. Özcan Yiğit is appreciated for careful editorial handling of the manuscript.

References

Aghajani Marsa S, Emami MH, Lotfi M, Gholizadeh K, Ghasemi Siani M (2015). Source of polymetal epithermal veins at Nikuyeh district (west of Qazvin) based on mineralogy, alteration and fluid inclusion studies. Scientific Quarterly Journal of Geosciences 25: 157–168 (in Persian with English abstract).

Amin Khorramdasht Exploration Company (2006). Final Report of Technical Services in Zehabad Pb-Zn Deposit. Internal Report. Tehran, Iran: Amin Khorramdasht Exploration Company (in Persian).

Annells RN, Arthurton RS, Bazley RA, Davie, RG (1975). Explanatory Text of the Qazvin and Rasht Quadrangles Map, E3 and E4. Tehran, Iran: Geological Survey of Iran.

Annells RS, Arthurton RS, Bazley RAB, Davies RG, Hamedi MAR et al. (1985). Geological Quadrangle Map of Qazvin-Rasht (1:250,000). Tehran, Iran: Geological Survey of Iran.

Asiabanha A, Foden F (2012). Post-collisional transition from an extensional volcano-sedimentary basin to a continental arc in the Alborz ranges, N-Iran. Lithos 148: 98-111.

Asiabanha A, Ghasemi H, Meshkin M (2009). Paleogene continental-arc type volcanism in north Qazvin, north Iran: facies analysis and geochemistry. Neues Jahrbuch für Mineralogie – Abhandlungen (Journal of Mineralogy and Geochemistry) 186 (2): 201-214.

Ballato P, Cifelli F, Heidarzadeh G, Ghassemi M, Wicker A et al. (2017). Tectono-sedimentary evolution of the northern Iranian Plateau: insights from middle-late Miocene foreland-basin deposits. Basin Research 29: 417-446.

Ballato P, Mulch A, Landgraf A, Strecker MR, Dalconi MC et al. (2010). Middle to late Miocene Middle Eastern climate from stable oxygen and carbon isotope data, southern Alborz Mountains, N Iran. Earth and Planetary Science Letters 300: 125-138.

Ballato P, Uba CE, Landgraf A, Strecher MR, Sudo M et al. (2011). Arabia-Eurasia continental collision: insights from late Tertiary foreland-basin evolution in the Alborz Mountains, northern Iran. Geological Society of America Bulletin 123: 106-131.

Bortnikov NS, Genkin AD, Dobrovol'skaya MG, Muravitskaya GN, Filimonova AA (1991). The nature of chalcopyrite inclusions in sphalerite: exsolution, coprecipitation, or "disease"? Economic Geology 86: 1070-1082.

Buchanan LJ (1981). Precious metal deposits associated with volcanic environments in the southwest. In: Dickinson WR, Payne WD (editors). Relations of Tectonics to Ore Deposits in the Southern Cordillera. Tucson, AZ, USA: Arizona Geological Society, pp. 237-262.

Castro A, Aghazadeh M, Badrzadeh Z, Chichorro M (2013). Late Eocene-Oligocene post-collisional monzonitic intrusions from the Alborz magmatic belt, NW Iran: an example of monzonite magma generation from a metasomatized mantle source. Lithos 180-181: 109-127.

Corbett GJ, Leach TM (1998). Southwest Pacific Rim Gold-Copper Systems: Structure, Alteration, and Mineralization (No. 6). Boulder, CO, USA: Society of Economic Geologists.

Einaudi MT, Hedenquist JW, Inan EE (2003). Sulfidation state of hydrothermal fluids: the porphyry-epithermal transition and beyond. In: Simmons SF, Graham IJ (editors). Volcanic, Geothermal and Ore-Forming Fluids: Rulers and Witnesses of Processes within the Earth. Tulsa, OK, USA: Society of Economic Geologists and Geochemical Society Special Publications, pp. 285-313.

Esmaeli M, Lotfi M, Nezafati N (2015). Fluid inclusion and stable isotope study of the Khalyfehlou copper deposit, southeast Zanjan, Iran. Arabian Journal of Geosciences 8 (11): 9625-9633.

Field C, Fifarek RH (1985). Light stable-isotope systematics in the epithermal environment. Reviews in Economic Geology 2: 99-128.

Fornadel AP, Voudoris PC, Spry PG, Melfos V (2012). Mineralogical, stable isotope and fluid inclusion studies of spatially related porphyry Cu and epithermal Au-Te mineralization, Fakos Peninsula, Limnos Island, Greece. Mineralogy and Petrology 105: 85-111.

Guest B, Axen GJ, Lam PS, Hassanzadeh J (2006). Late Cenozoic shortening in the west-central Alborz Mountains, northern Iran, by combined conjugate strike-slip and thin-skinned deformation. Geosphere 2 (1): 35-52.

Gülyuz N, Shipton ZK, Kuşcu I, Lord RA, Kaymakcı N et al. (2018). Repeated reactivation of clogged permeable pathways in epithermal gold deposits: Kestanelik epithermal vein system, NW Turkey. Journal of the Geological Society 175: 509-524.

Hanilçi N, Bozkaya G, Banks D, Prokoviev V, Oztas Y (2015). Preliminary microthermometric data from the Kisladag Au deposit, western Turkey: porphyry/porphyry-epithermal transition? In: European Current Research on Fluid Inclusions (ECROFI-XXIII); Leeds, ; UK; June 2015. Extended Abstracts Volume, pp. 75-76.

Hedenquist JW, Arribas AJR, Gonzalez-Urien E (2000). Exploration for epithermal gold deposits. Reviews in Economic Geology 13: 245-277.

Heinrich CA, Neubauer F (2002). Cu-Au-Pb-Zn-Ag metallogeny of the Alpine-Balkan-Carpathian-Dinaride geodynamic province. Mineralium Deposita 37: 533-540.

Henley RW (1984). Hydrolysis reactions in hydrothermal fluids. Reviews in Economic Geology 1: 65-82.

Henley RW, Ellis AJ (1983). Geothermal systems ancient and modern: a geochemical review. Earth-Science Reviews 19: 1-50.

Hoefs J (2009). Stable Isotope Geochemistry. Berlin, Germany: Springer-Verlag.

Imer A, Richards JP, Creaser RA (2013). Age and tectonomagmatic setting of the Eocene Çöpler–Kabataş magmatic complex and porphyry-epithermal Au deposit, East Central Anatolia, Turkey. Mineralium Deposita 48: 557-583.

Imer A, Richards JP, Muehlenbachs K (2016). Hydrothermal evolution of the Çöpler porphyry-epithermal Au deposit, Erzincan province, central Eastern Turkey. Economic Geology 111: 1619-1658.

Jahandideh Kazempour K, Hosseini M, Hakimi Asiabar S (2011). The study of mineralization in the Abbas Abad polymetallic ore deposit (northwestern Qazvin province, Iran). Quarterly Journal of Earth Resources 4 (3): 21-32 (in Persian).

Khodaparast S (2002). Survey of controlling factors in mineralization at Zehabad polymetallic deposit (north of Abhar). MSc, Islamic Azad University, North Tehran Branch, Iran (in Persian with English abstract).

Kouhestani H, Ghaderi M, Chang Z, Zaw K (2015). Constraints on the ore fluids in the Chah Zard breccia-hosted epithermal Au–Ag deposit, Iran: fluid inclusions and stable isotope studies. Ore Geology Reviews 65: 512-521.

Kouhestani H, Ghaderi M, Zaw K, Meffre S, Emami MH (2012). Geological setting and timing of the Chah Zard breccia hosted epithermal gold-silver deposit in the Tethyan belt of Iran. Mineralium Deposita 47: 425-440.

Kouhestani H, Mokhtari MAA (2017). Mineralization and fluid evolution of epithermal base metal veins from the Aqkand deposit, NW Iran. Neues Jahrbuch für Mineralogie – Abhandlungen (Journal of Mineralogy and Geochemistry) 194 (2): 139-155.

Kouhestani H, Mokhtari MAA, Chang Z, Johnson CA (2018). Intermediate sulfidation type base metal mineralization at Aliabad-Khanchy, Tarom-Hashtjin metallogenic belt, NW Iran. Ore Geology Reviews 93: 1-18.

Leach T, Corbett G (2008). Fluid mixing as a mechanism for bonanza grade epithermal gold formation. In: Terry Leach Symposium; Sydney, Australia.

Madanipour S (2013). Spatial and temporal pattern of exhumation in the Talesh Mountain, NW Iran. PhD, Tarbiat Modares University, Tehran, Iran (in Persian with English abstract).

Malekzadeh-Shafaroudi A, Karimpour MH (2015). Mineralogic, fluid inclusion, and sulfur isotope evidence for the genesis of Sechangi lead-zinc (–copper) deposit, eastern Iran. Journal of African Earth Sciences 107: 1-14.

McKibben MS, Eldridge CS (1990). Radical sulfur isotope zonation of pyrite accompanying boiling and epithermal gold deposition: a SHRIMP study of the Valles Caldera, New Mexico. Economic Geology 85: 1917-1925.

Mehrabi B, Ghasemi Siani M, Goldfarb R, Azizi H, Ganerod M et al. (2016). Mineral assemblages, fluid evolution, and genesis of polymetallic epithermal veins, Glojeh district, NW Iran. Ore Geology Reviews 78: 41-57.

Mohammadi-Niaei R, Daliran F, Nezafati N, Ghorbani M, Sheikh-Zakariaei J et al. (2015). The Ay Qalasi deposit: an epithermal Pb–Zn (Ag) mineralization in the Urumieh–Dokhtar volcanic belt of northwestern Iran. Neues Jahrbuch für Mineralogie – Abhandlungen (Journal of Mineralogy and Geochemistry) 192 (3): 263-274.

Moradi M (2011). Genesis of Cu and Pb mineralization at Abbas Abad, Tarom Sofla, Qazvin. MSc, Sistan and Baluchestan University, Zahedan, Iran (in Persian with English abstract).

Moradi M, Boomeri M, Maanijou M, Hosseini M (2010). Geology and mineralogy in Abbas Abad Pb-Cu-Zn deposit, NW Iran. In: The First Congress of the Iranian Society of Economic Geology.

Nabatian G, Ghaderi M, Neubauer F, Honarmand M, Xiaoming L et al. (2014). Petrogenesis of Tarom high-potassic granitoids in the Alborz-Azarbaijan belt, Iran: geochemical, U-Pb zircon and Sr-Nd–Pb isotopic constraints. Lithos 184-187: 324-345.

Nabatian G, Jiang SY, Honarmand M, Neubauer F (2016). Zircon U-Pb ages, geochemical and Sr-Nd-Pb-Hf isotopic constraints on petrogenesis of the Tarom-Olya pluton, Alborz magmatic belt, NW Iran. Lithos 244: 43-58.

Nabavi MH (1976). Introduction to Geology of Iran. Tehran, Iran: Geological Survey of Iran.

Ohmoto H (1972). Systematics of sulfur and carbon isotopes in hydrothermal ore deposits. Economic Geology 67: 551-579.

Ohmoto H, Rye RO (1979). Isotopes of sulfur and carbon. In: Barnes HL (editor). Geochemistry of Hydrothermal Ore Deposits. New York, NY, USA: John Wiley and Sons, pp. 509-567.

Poliquin M (2004). Low-Sulfidation Epithermal Quartz-Adularia Gold-Silver Veins & the El Fuego Project, Mexico. Vancouver, Canada: Almaden Minerals Ltd.

Rajabpour S, Behzadi M, Jiang SY, Rasa I, Lehmann B et al. (2017). Sulfide chemistry and sulfur isotope characteristics of the Cenozoic volcanic-hosted Kuh-Pang copper deposit, Saveh county, northwestern central Iran. Ore Geology Reviews 86: 563-583.

Reyes AG (1990). Petrology of Philippine geothermal systems and the application of alteration mineralogy to their assessment. Journal of Volcanology and Geothermal Research 43: 279-309.

Richards JP (2009). Post-subduction porphyry Cu-Au and epithermal Au deposits: products of remelting of subduction-modified lithosphere. Geology 37 (3): 247-250.

Rye RO (1993). Evolution of magmatic fluids in the epithermal environment: the stable isotope perspective. Economic Geology 88: 733-753.

Seal RR, Rye RO (1992). Stable isotope of water-rock interaction and ore formation, Bayhorse base and precious metal district, Idaho, USA. Economic Geology 87: 271-287.

Shahbazi S, Ghaderi M (2014). Zehabad gold mineralization, an example of epithermal deposits related to high-potassium magmatism in post-subduction extension environment. In: 18th Symposium of the Geological Society of Iran (in Persian).

Shahbazi S, Ghaderi M, Madanipour S (2018). The role of Zanjan-Manjil semi-brittle zone in controlling the Zehabad Pb, Zn, Au, Ag (Cu) mineralization, NW Qazvin. In: 36th National and the 3rd National Geosciences Congress (in Persian with English abstract).

Sherlock RL, Tosdal RM, Lehman NJ, Graney JR, Losh S et al. (1995). Origin of the McLaughlin mine sheeted vein complex: metal zoning, fluid inclusion and isotopic evidence. Economic Geology 90: 2156-2181.

Sillitoe RH (2010). Porphyry copper systems. Economic Geology 105: 3-41.

Sillitoe RH, Hedenquist JW (2003). Linkages between volcanotectonic settings, ore-fluid compositions, and epithermal precious metal deposits. Economic Geology Special Publications 10: 315-343.

Sillitoe RH, Tolma J, Van Kerkvoort G (2013). Geology of the Caspiche porphyry gold-copper deposit, Maricunga belt, northern Chile. Economic Geology 108: 585-604.

Simmons SF, Browne PRL (2000). Hydrothermal minerals and precious metals in the Broadlands-Ohaaki geothermal system: implications for understanding low-sulfidation epithermal environments. Economic Geology 95: 971-999.

Simmons SF, Christenson BW (1994). Origins of calcite in a boiling geothermal system. American Journal of Science 294: 361-400.

Stocklin J, Eftekharnezhad J (1969). Explanatory text of the Zanjan Quadrangle Map. Tehran, Iran: Geological Survey of Iran.

Thompson AJB, Thompson JFH (1998). Atlas of Alteration: A Field Guide to Hydrothermal Alteration Minerals. Vancouver, Canada: Alpine Press Ltd.

Verdel C, Wernicke BP, Hassanzadeh J, Gues B (2011). A Paleogene extensional arc flare-up in Iran. Tectonics 30: 1-20.

Vincent SJ, Allen MB, Ismail-Zadeh AD, Flecker R, Foland KA et al. (2005). Insights from the Talysh of Azerbaijan into the Paleogene evolution of the South Caspian region. Bulletin of the Geological Society of America 117: 1513-1533.

Wang L, Qin KZ, Song GX, Li GM (2019). A review of intermediate sulfidation epithermal deposits and subclassification. Ore Geology Reviews 107: 434-456.

Yasami N, Ghaderi M, Alfonso P (2018). Sulfur isotope geochemistry of the Chodarchay Cu-Au deposit, Tarom, NW Iran. Neues Jahrbuch für Mineralogie – Abhandlungen (Journal of Mineralogy and Geochemistry) 195 (2): 1-13.

Yasami N, Ghaderi M, Madanipour S, Taghilou B (2017). Structural control on overprinting high-sulfidation epithermal on porphyry mineralization in the Chodarchay deposit, northwestern Iran. Ore Geology Reviews 86: 212-224.

Yilmaz H, Oyman T, Arehart GB, Colakoglu AR, Billor Z (2007). Low-sulfidation type Au-Ag mineralization at Bergama, Izmir, Turkey. Ore Geology Reviews 32: 81-124.

Yilmaz H, Oyman T, Sonmez FN, Arehart GB, Billor Z (2010). Intermediate sulfidation epithermal gold-base metal deposits in Tertiary subaerial volcanic rocks, Sahinli/Tespih Dere (Lapseki/western Turkey). Ore Geology Reviews 37: 236-258.

Zanchi A, Berra F, Mattei M, Ghassemi M, Sabouri J (2006). Inversion tectonics in Central Alborz, Iran. Geology 28: 2023-2037.